

DualCross: Cross-Modality Cross-Domain Adaptation for Monocular BEV Perception

Yunze Man
UIUC

yunzem2@illinois.edu

Liang-Yan Gui
UIUC

lgui@illinois.edu

Yu-Xiong Wang
UIUC

yxw@illinois.edu

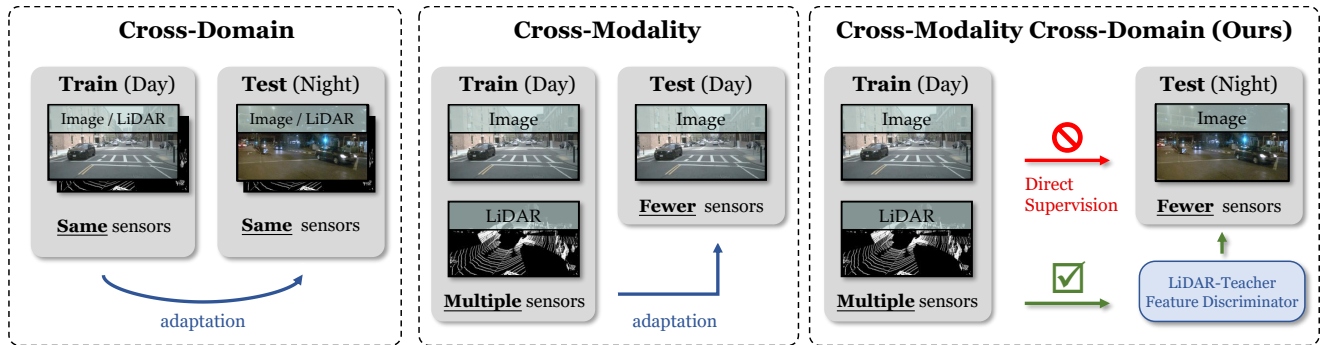


Figure 1: *Left & Middle:* Existing adaptation models assume either a fixed modality or a fixed domain between training and testing phases. *Right:* A more realistic setting considers both cross-modality and cross-domain shifts. We propose DualCross to reduce the domain and modality discrepancy, and achieve state-of-the-art performance.

Abstract

Closing the domain gap between training and deployment and incorporating multiple sensor modalities are two challenging yet critical topics for self-driving. Existing work only focuses on single one of the above topics, overlooking the simultaneous domain and modality shift which pervasively exists in real-world scenarios. A model trained with multi-sensor data collected in Europe may need to run in Asia with a subset of input sensors available. In this work, we propose DualCross, a cross-modality cross-domain adaptation framework to facilitate the learning of a more robust monocular bird’s-eye-view (BEV) perception model, which transfers the point cloud knowledge from a LiDAR sensor in one domain during the training phase to the camera-only testing scenario in a different domain. This work results in the first open analysis of cross-domain cross-sensor perception and adaptation for monocular 3D tasks in the wild. We benchmark our approach on large-scale datasets under a wide range of domain shifts and show state-of-the-art results against various baselines. Our project webpage is at <https://yunzeman.github.io/DualCross>.

1. Introduction

In recent years, multi-modality 3D perception has shown outstanding performance and robustness over its single-modality counterpart, achieving leading results for various 3D perception tasks [14, 23, 27, 31, 36, 42] on large-scale multi-sensor 3D datasets [3, 15, 34]. Despite the superiority in information coverage, the introduction of more sensor modalities also poses additional challenges to the perception system. On one hand, generalizing the model between datasets becomes hard, because each sensor has its unique properties, such as field-of-view (FoV) for cameras, density for LiDAR, etc. On the other hand, the operation of the model is conditioned on the presence and function of more sensors, making it hard to work on autonomous agents with less sensor types or under sensor failure scenarios.

More specifically, transferring knowledge among different data domains is still an open problem for autonomous agents in the wild. In the self-driving scenario, training the perception models offline in a source domain with annotation while deploying the model in a different target domain without annotation is very common in practice. As a result, a model has to consider the domain gap between source and target environments or datasets, which usually involves different running locations, different sensor specifications, dif-

ferent illumination and weather conditions, *etc.*

Meanwhile, in addition to domain shift, modality shift is another factor which challenges the successful deployment of models. The widely adopted assumption that all sensors are available during training, validation, and deployment time is not always true in reality. Due to the cost and efficiency trade-off, or sensor missing and failure, in many scenarios we can have fewer sensors available in the target domain during testing than what we have in the source domain during training. A typical scenario is having camera and LiDAR sensors in the large-scale training phase while only having cameras for testing, as shown in Figure 1. It is not clear how to facilitate the camera-only 3D inference with the help of a LiDAR sensor only in the source domain during training.

The challenges above raise an important question: *Can we achieve robust 3D perception under both domain shift and sensor modality shift?* Existing methods either study cross-domain scenarios assuming consistent modality [10, 14, 17, 20, 22, 29, 32, 47, 49], or study cross-modality scenarios assuming the same domain during training and validation [6, 8, 11, 13, 18, 19, 46]. However, simultaneous domain and modality shift poses additional challenges of large domain discrepancy and exacerbates the ill-pose nature of 3D inference from monocular information due to the misaligned sensory data. As we will discuss in Sec. 3.2, our new problem setting requires a novel methodology in using LiDAR without increasing the domain discrepancy.

To tackle the above challenges, we propose DualCross, a cross-modality cross-domain adaptation framework for bird’s-eye-view (BEV) perception. Our model addresses the monocular 3D perception task between different domains, and utilizes additional modalities in the source domain to facilitate the evaluation performance. Motivated by the fact that image and BEV frames are bridged with 3D representation, we first design an efficient backbone to perform 3D depth estimation followed by a BEV projection. Then, to learn from point clouds without explicitly taking them as model inputs, we propose an implicit learning strategy, which distills 3D knowledge from a LiDAR-Teacher to help the Camera-Student learn better 3D representation. Finally, in order to address the visual domain shift, we introduce adversarial learning on the student to align the features learned from source and target domains. Supervision from the teacher and feature discriminators are designed at multiple layers to ensure an effective knowledge transfer.

By considering the domain gap and effectively leveraging LiDAR point clouds in the source domain, our proposed method is able to work reliably in more complicated, uncommon, and even unseen environments. Our model achieves state-of-the-art performance in four very different domain shift settings. Extensive ablation studies are conducted to investigate the contribution of our proposed com-

ponents, the robustness under different changes, and other design choices.

The main contributions of this paper are as follows. (1) We introduce mixed domain and modality mismatch, an overlooked but realistic problem setting in 3D domain adaptation in the wild, leading to a robust camera-only 3D model that works in complicated and dynamic scenarios with minimum sensors available. (2) We propose a novel LiDAR-Teacher and Camera-Student knowledge distillation model, which considerably outperforms state-of-the-art LiDAR supervision methods. (3) Extensive experiments in challenging domain shift settings demonstrate the capability of our methods in leveraging source domain point cloud information for accurate monocular 3D perception.

2. Related Work

Multi- and Cross-modality 3D Perception. Considerable research has examined leveraging signals from multiple modalities, especially images and point clouds, for 3D perception tasks. Early work [21] projects point clouds to the BEV frame and fuses 2D RGB features to generate proposals and regress bounding boxes. Later work [48, 51] explores deep fusion between points and images. Under the umbrella of the cross-modality setting, 2DPASS [46] transfers features learned from images to the LiDAR. BEVDepth [19] obtains reliable depth estimation by exploiting camera parameters with image features during training. More recently, a line of work explores knowledge distillation from one sensor to another for 3D object detection [6, 8, 11, 13, 18, 19, 46]. On the contrary, our method explores a more realistic yet challenging setting, where we use LiDAR data in one domain (Boston/Sunny/Daylight) during training to help the camera-only model during inference in another domain (Singapore/Rainy/Night). As a result, we analyze and improve the actual usefulness of additional sensors under domain shift settings.

Cross-domain 3D Perception. While extensive research has been conducted on domain adaptation for 2D tasks, the field of domain adaptation for 3D perception in the real world has received relatively less attention. Some prior work adapts depth estimation from synthetic to real image domains [17, 50]. Working on point clouds, PointDAN [32] designs a multi-scale adaptation model for 3D classification. For 3D semantic segmentation, SqueezeSeg [43] projects point clouds to the 2D view, while other work [10, 14, 29] leverages point clouds and images data together. Recent work [22, 47, 49] explores cross-domain 3D object detection from point clouds. SRDAN [49] employs adversarial learning to align the features between different domains. Although prior work [14, 20] explores various domain adaptation techniques for different sensor modalities, these methods only adopt the same modalities to learn

the domain shift between source and target data. In contrast, our approach achieves robust 3D perception in a more general scenario, where the model can perform accurate 3D inference in the target domain by adapting information encoded in source-exclusive modalities.

3D Inference in Bird’s-Eye-View Frame. Inferring 3D scenes from the BEV perspective has recently received a large amount of interest due to its effectiveness. MonoLayout [24] estimates the layout of urban driving scenes from images in the BEV frame and uses an adversarial loss to enhance the learning of hidden objects. Another work [4] proposes to employ graphical representation and temporal aggregation for better inference in the driving scenarios using on-board cameras. Recently, using BEV representation to merge images from multiple camera sensors has become a popular approach [12, 26]. Following the monocular feature projection proposed by Orthographic Feature Transform (OFT) [33], Lift-Splat-Shoot [30] disentangles feature learning and depth inference by learning a depth distribution over pixels to convert camera image features into BEV. Unlike the above work performing BEV analysis in settings with more controlled premises, we are the first to explore cross-domain and cross-sensor settings, leading to a more robust and more realistic 3D inference methodology.

3. Approach

In this work, we consider the task of learning BEV representation of scenes with domain shift and modality mismatch. Specifically, the model will be given annotated LiDAR point clouds and camera images in the source domain, but only unannotated camera images in the target domain. And the model seeks to achieve highest performance on the unsupervised target domain. This problem setting is common and worthwhile, especially considering the existence of many existing public multi-modality datasets and the rise of many camera-only vehicle scenarios.

Formally, **for the source domain**, we are given *labeled* data with N^s multi-modality samples, $\mathcal{D}^s = \{(\mathbf{X}_i^s, \mathbf{P}_i^s, \mathbf{y}_i^s)\}_{i=1}^{N^s}$, where s represents the source domain. Here $\mathbf{X}_i^s = \{\mathbf{x}_{ik}^s\}_{k=1}^n$ consists of n camera images $\mathbf{x}_{ik}^s \in \mathbb{R}^{3 \times H \times W}$. The number of cameras n can take any integer as small as one, depending on the dataset or cameras deployed on the vehicle. In addition, each camera image has an intrinsic matrix and an extrinsic matrix. \mathbf{P}_i^s is a point cloud containing multiple unordered points $\mathbf{p} \in \mathbb{R}^3$ represented by 3D coordinate values. And label \mathbf{y}_i^s represents rasterized representation of the scenes in the BEV coordinate. **For the target domain**, we are given *unlabeled* data with N^t image samples, $\mathcal{D}^t = \{\mathbf{X}_i^t\}_{i=1}^{N^t}$, where t represents the target domain, and we want to estimate $\{\mathbf{y}_i^t\}_{i=1}^{N^t}$, the BEV representation of the scenes in the target domain.

An overview of our method DualCross is illustrated in

Figure 2. DualCross is designed to extract features from monocular images and project the features into the BEV frame (Section 3.1), using estimated or ground truth 3D depth information. The model is composed of a LiDAR-teacher and a Camera-student (Section 3.2), where the teacher encodes how to learn better representation given point clouds, and transfers that knowledge to the camera-only student using multi-level teacher-student supervision. Finally, to bridge the domain gap between source and target domains, we leverage adversarial discriminators at different feature layers to align the distributions across two domains in the camera-student model (Section 3.3). Finally, we describe the overall learning objective and loss designs (Section 3.4).

3.1. Learning BEV from Images

In order to achieve 3D perception under the cross-modality setting, our first challenge is to unify the image coordinates, point cloud coordinates, and BEV coordinates into a joint space. We follow LSS [30] to transform the image features from perspective view into the BEV view. Specifically, we tackle this problem by constructing a 3D voxel representation of the scene for each input image. We discretize the depth axis into N_d bins and lift each pixel of the images into multiple voxels (frustums), where each voxel is represented by the 3D coordinate of its center location. For a given pixel $\text{px} = (h, w)$ on one of the camera image, it corresponds to a set of N_d voxels at different depth bins:

$$V_{\text{px}} = \{v_i = M^{-1}[d_i h, d_i w, d_i]^T | i \in \{1, 2, \dots, N_d\}\}, \quad (1)$$

where M is camera matrix and d_i is the depth of the i -th depth bin. The feature vector of each voxel v_i in V_{px} is the base feature \mathbf{f}_{px} of pixel px scaled by the depth value α_i . More specifically, $\mathbf{f}_{v_i \in V_{\text{px}}} = \alpha_i \cdot \mathbf{f}_{\text{px}}$, where the pixel feature \mathbf{f}_{px} is extracted by an image encoder. And the depth value α_i is obtained either from LiDAR point clouds or by estimation, in the teacher and student model, respectively. The acquirement of α_i is introduced in Sec. 3.2.

After getting the feature for each of the voxels, we project the voxels onto the BEV and aggregate the features to get the BEV feature map. The BEV frame is rasterized into (X, Y) 2D grids, and for each grid, its feature is constructed from the features of all the 3D voxels projected into it using mean pooling. This projection allows us to transform an arbitrary number of camera images into a unified BEV frame. Finally, we obtain an image-like BEV feature embedding, which is used to estimate the final representation using a convolutional neural network (CNN) decoder.

This architecture design bridges the image and LiDAR modalities through an intermediate 3D voxelized representation. Hence, we can take LiDAR point clouds as input into the model to directly guide the BEV projection without hav-

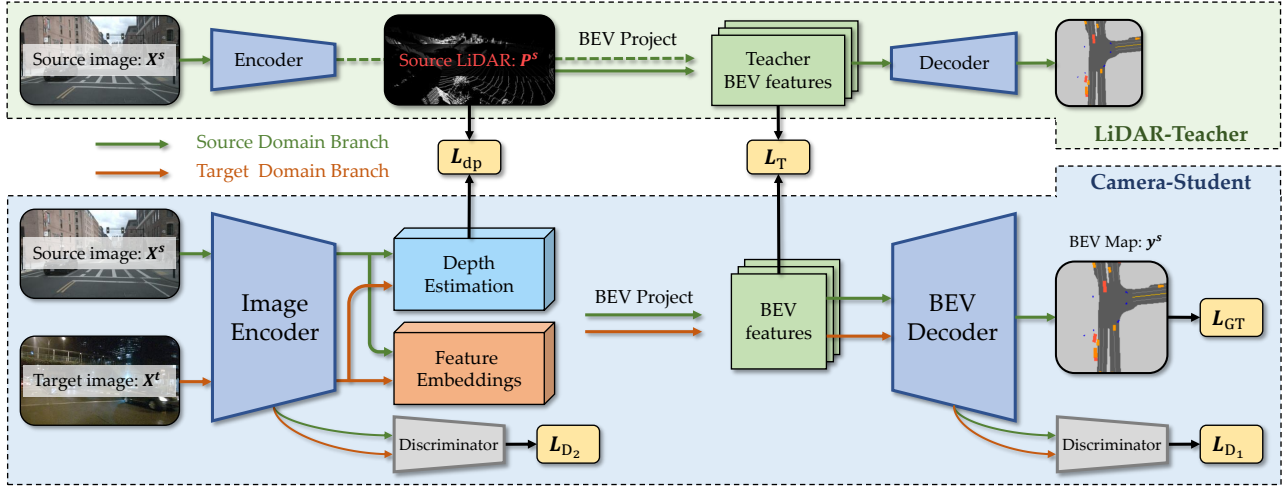


Figure 2: **Overview of our DualCross framework.** DualCross includes three components. (1) **LiDAR-Teacher** uses voxelized LiDAR point clouds to transform the image features to the BEV frame. It provides essential knowledge on how to guide image learning given LiDAR information. (2) **Camera-Student** is supervised by the teacher model as well as the LiDAR ground truth. (3) **Discriminators** are used to align features from source and target domains.

ing to change the overall pipeline. This further enables the distillation of knowledge from the point clouds to images using a teacher-student model.

3.2. LiDAR-Teacher and Camera-Student

The co-existence of domain and modality gaps poses additional challenges to the adaptation task. Although the LiDAR sensor in the source domain provides 3D knowledge to the model, it also increases the discrepancy between the two domains, which hurts the model adaptation (as we will see in Sec. 4.2 and Table 4). Hence, the unique difficulty of our work lies in exploiting the *LiDAR point clouds* during training to guide the camera model for better 3D estimation.

Depth Supervision by Point Clouds. The main advantage of point clouds over the image modality is the accurate 3D positional information coming from the depth measurement. Due to the lack of LiDAR during evaluation, we cannot use point clouds as direct input of the model. Hence, one alternative approach to using point clouds is to supervise the depth estimation in the model. As in Eq. 1, for each pixel, we calculate the features of its corresponding voxels by multiplying the pixel feature with a depth value α_i . We use another head to predict a depth distribution $\alpha_{px} = \{\alpha_1, \alpha_2, \dots, \alpha_{N_d}\}$ over N_d depth bins for each pixel px .

The ground truth depth supervision for this estimation task is generated by LiDAR point clouds as follows: When projected to the image frame, the points corresponding to one pixel can have three conditions. If the pixel has, (1) **no point inside**: the ground truth depth distribution of it is omitted; (2) **only one point inside**: the ground truth depth distribution is a one-hot vector, with value one being in the

voxel that the point lies in; (3) **multiple points inside**: the ground truth depth distribution α_i of this point is calculated by counting the number of points in each depth bin, and dividing them by V_{px} , the total number of points in α_{px} :
$$\alpha_i = \frac{\text{Number of points in depth bin } v_i}{\text{Total number of points in } V_{px}}.$$

Using a distribution-based depth representation effectively accounts for the ambiguity when objects of different depth occur in one pixel. This happens at the boundary of the objects, and becomes more severe during feature encoding processing when images get down-sampled and each pixel represents larger space. Moreover, a probabilistic depth representation considers uncertainty during depth estimation, and degenerates to pseudo-LiDAR methods [41] if the one-hot constraint is added.

Learning from LiDAR-Teacher. Despite being intuitive and straightforward, direct depth supervision is not optimal for two reasons. First, LiDAR supervision is only on the intermediate feature layer, providing no supervision on the second half of the model. Also, while LiDAR provides accurate depth measurement, “depth estimation” is still different from our overall objective on BEV representation. Motivated by this, as shown in Figure 2, we propose to use a pretrained LiDAR oracle model to supervise the image model at the final BEV feature embedding, such that the supervision of LiDAR is provided to the whole model and aligns better with the final objective. We call the model using ground truth point cloud information “LiDAR-Teacher,” and the model to be supervised “Camera-Student.” This boils down to a knowledge distillation problem where the 3D inference knowledge of the LiDAR-teacher is distilled to the camera-only student. Note that the classic problem

of “better teacher, worse student” [7, 25, 52] in knowledge distillation due to capacity mismatch does not exist in this model, because the LiDAR-Teacher and Camera-Student models in DualCross are almost identical.

Overall, this teacher-student mechanism allows the camera model to learn better 3D representation from the point clouds, leading to better LiDAR supervision at different stages, while still keeping the model image-centric for image-only inference.

3.3. Cross-Domain Adaptation

Since the BEV annotations and the LiDAR ground truth are only available in the source data, the model will be heavily biased to the source distribution during teacher-student supervision. Hence, we bridge the target and source domains using adversarial training. Specifically, we place one discriminator D_1 at the BEV decoder CNN blocks, and another D_2 at the image encoder CNN blocks, to align the features of two domains by optimizing over discriminator losses. While the final-layer discriminator D_1 is constantly useful to align features learned from the LiDAR-Teacher and final ground truth, we find that the middle-layer discriminator D_2 is very effective under certain domain gaps where images have great changes but LiDAR remains robust.

To achieve adversarial learning, given a feature encoder E and input sample X , a domain discriminator D is used to discriminate whether the feature $E(X)$ comes from the source domain or the target domain. The target and source domain samples are given the label $d = 1$ and $d = 0$, respectively. And $D(E(X))$ outputs the probability of the sample X belonging to the target domain. Hence, the discriminator loss is formulated by a cross-entropy loss:

$$\mathcal{L}_{\text{dis}} = d \log D(E(X)) + (1 - d) \log(1 - D(E(X))). \quad (2)$$

Moreover, in order to learn domain-invariant features, our feature encoder E should try to extract features that fool the discriminator D , while the discriminator D tries to distinguish the right domain label of the samples. This adversarial strategy can be formulated as a “min-max” optimization problem: $\mathcal{L}_D = \min_E \max_D \mathcal{L}_{\text{dis}}$. The “min-max” problem is achieved by a Gradient Reverse Layer (GRL) [9], which produces reverse gradient from the discriminator D to learn the domain-invariant encoder E . The loss form is the same for both D_1 and D_2 .

3.4. Full Objective and Inference

The overall objective of our model is composed of the supervision from the BEV ground truth, the LiDAR-Teacher, and the domain alignment discriminators. Given the output rasterized BEV representation map $\mathbf{y} \in \mathbb{R}^{X \times Y \times C}$, the ground truth (GT) loss term \mathcal{L}_{GT} can be formulated as a cross-entropy loss between the estimated source domain BEV map $\tilde{\mathbf{y}}^s$ and the GT label \mathbf{y}^s :

$$\mathcal{L}_{\text{GT}}(\tilde{\mathbf{y}}^s, \mathbf{y}^s) = - \sum_{i=1}^X \sum_{j=1}^Y \sum_{k=1}^C y_{(i,j,k)}^s \log \tilde{y}_{(i,j,k)}^s. \quad (3)$$

The supervision from the LiDAR-Teacher is composed of a direct depth estimation loss \mathcal{L}_{dp} and a teacher feature supervision \mathcal{L}_T . As described in Sec. 3.1, given the 3D depth volume $\alpha \in \mathbb{R}^{H \times W \times N_d}$, the direct depth supervision term \mathcal{L}_{dp} is formulated as a cross-entropy loss between the estimated 3D depth distribution volume $\tilde{\alpha}^s$ in the source domain, and the GT depth volume α^s calculated from LiDAR point clouds as described in Sec. 3.2:

$$\mathcal{L}_{\text{dp}}(\tilde{\alpha}^s, \alpha^s) = - \sum_{i=1}^H \sum_{j=1}^W \sum_{k=1}^{N_d} \alpha_{(i,j,k)}^s \log \tilde{\alpha}_{(i,j,k)}^s. \quad (4)$$

And for the LiDAR-Teacher feature supervision: $\mathcal{L}_T(\mathbf{F}^{\text{te}}, \mathbf{F}^{\text{st}}) = \mathcal{L}_2(\mathbf{F}^{\text{te}}, \mathbf{F}^{\text{st}})$ is an \mathcal{L}_2 loss, where \mathbf{F}^{te} and \mathbf{F}^{st} are the feature maps of teacher and student models, respectively. Finally, the domain adaptation loss contains \mathcal{L}_{D_1} and \mathcal{L}_{D_2} with the form described in Eq. 2.

The final objective is formulated as a multi-task optimization problem:

$$\mathcal{L}_{\text{DualCross}} = \mathcal{L}_F + \lambda_T \mathcal{L}_T + \lambda_{\text{dp}} \mathcal{L}_{\text{dp}} + \lambda_{D_1} \mathcal{L}_{D_1} + \lambda_{D_2} \mathcal{L}_{D_2}, \quad (5)$$

where $\lambda_T, \lambda_{\text{dp}}, \lambda_{D_1}$, and λ_{D_2} are weights for the corresponding loss terms. The DualCross model is trained end-to-end using the loss term in Eq. 5. During inference, target samples are fed into the Camera-Student model to output the final BEV representation. More training details are provided in Sec. 4.

4. Experiments

Datasets and Domain Settings. We evaluate DualCross with four unique domain shift settings constructed from two large-scale datasets, nuScenes [3] and Lyft [15], following existing LiDAR-based domain adaptation work, including SRDAN [49], ST3D [47], UDA3D [22], and xMUDA [14]. Specifically, for the *day-to-night*, *city-to-city*, and *dry-to-rain* settings, we use the sentence in the nuScenes dataset and filter the keywords to split the dataset into corresponding subsets to create the intra-class adaptation scenarios. For the *dataset-to-dataset* setting, we use the official split of the nuScenes dataset, and the split provided in ST3D [47] for the Lyft dataset. All adaptation settings follow the assumption that the source has access to cameras and LiDAR sensors, while the target only has cameras. We use all six cameras provided by the nuScenes dataset. We also analyze surprising observations on cross-modality performance in the ablation study.

Implementation Details. Following [30], we use EfficientNet [35] pretrained on ImageNet as our image encoder backbone. Two heads are applied to estimate pixel fea-

Table 1: DualCross leads to significant improvements under *day-to-night* and *dry-to-rain* domain shift settings. Numbers reported in IoU. *DA* and *CM* denote whether a model considers domain adaptation and cross-modality in design, respectively.

Day → Night	<i>DA</i>	<i>CM</i>	Vehicle	Road	Lane
MonoLayout [24]	✗	✗	5.9	37.7	5.9
OFT [33]	✗	✗	6.6	40.5	6.0
LSS [30]	✗	✗	6.7	41.2	7.1
Wide-range Aug.	✓	✗	10.3	46.0	10.4
Vanilla DA	✓	✗	11.2	48.8	11.1
Depth-Supv DA	✓	✓	15.7	50.5	14.2
Input-fusion Teacher	✓	✓	14.9	48.8	13.1
DualCross (ours)	✓	✓	17.0	51.8	16.9

Dry → Rain	<i>DA</i>	<i>CM</i>	Vehicle	Road	Lane
MonoLayout [24]	✗	✗	20.6	68.7	13.1
OFT [33]	✗	✗	24.1	79.8	16.2
LSS [30]	✗	✗	27.8	71.0	16.8
Wide-range Aug.	✓	✗	28.2	71.2	17.2
Vanilla DA	✓	✗	29.1	70.8	18.3
Depth-Supv DA	✓	✓	29.6	71.8	19.1
Input-fusion Teacher	✓	✓	29.5	71.0	18.8
DualCross (ours)	✓	✓	29.6	71.9	19.5

Table 2: DualCross performs the best under *city-to-city* shift.

Boston → Singapore	<i>DA</i>	<i>CM</i>	Vehicle	Road	Lane
MonoLayout [24]	✗	✗	14.2	35.9	7.5
OFT [33]	✗	✗	16.8	37.9	9.6
LSS [30]	✗	✗	17.6	38.2	10.6
Wide-range Aug.	✓	✗	17.9	40.5	12.4
Vanilla DA	✓	✗	13.0	31.4	9.1
Depth-Supv DA	✓	✓	19.0	42.8	14.9
Input-fusion Teacher	✓	✓	18.6	42.7	14.1
DualCross (ours)	✓	✓	20.5	43.1	15.6

Table 3: DualCross performs the best under *dataset-to-dataset* domain gaps in IoU.

nuScenes → Lyft	<i>DA</i>	<i>CM</i>	Vehicle
MonoLayout [24]	✗	✗	11.8
OFT [33]	✗	✗	16.5
LSS [30]	✗	✗	19.9
Wide-range Aug.	✓*	✗	21.9
Vanilla DA	✓	✗	22.5
Depth-Supv DA	✓	✓	23.4
Input-fusion Teacher	✓	✓	22.8
DualCross (ours)	✓	✓	24.4

tures and pixel-wise depth distribution from the $8 \times$ down-sampled feature map. The 3D feature maps are projected to the BEV frame using mean pooling. For the BEV decoder we use ResNet-18 as the backbone, and upsample the features learned from the first three meta-layers of ResNet to the final BEV output. The D_1 and D_2 domain discriminators are applied to the output feature layers of EfficientNet and ResNet backbones, respectively. We use a light-weight discriminator architecture, which is composed of a global averaging pooling layer, followed by two fully-connected layers, and outputs the domain label. For input, we resize and crop input images to size 128×352 . For output, we consider a 100 meters \times 100 meters range centered at the ego-vehicle, with the grid size set to be 0.5 meters \times 0.5 meters. The depth bin is set to be 1.0 meter between 4.0 meters and 45.0 meters range. The whole model is trained end-to-end, with $\lambda_T = 1.0$, $\lambda_{dp} = 0.05$, $\lambda_{D_1} = 0.1$, $\lambda_{D_2} = 0.01$. We train DualCross using the Adam [16] optimizer with learning rate 0.001 and weight decay $1e-7$ for 50K steps for the teacher model, and 200K for the student model. We use horizontal flipping, random cropping, rotation, and color jittering augmentation during training. The whole model is implemented using the PyTorch framework [28].

4.1. BEV Segmentation Results and Comparisons

Baselines. We compare our method with state-of-the-art BEV 3D layout perception work MonoLayout [24], OFT [33], LSS [30], as well as other baseline methods in domain adaptation and cross-modality learning. *Wide-range Aug.* means using a wide range of random scaling

augmentation which potentially includes the target domain scale. For *Vanilla DA*, we adapt camera-only DA-Faster [5] to our BEV perception setting. *Depth-Supv DA* stands for depth-supervised domain adaptation. We use source domain LiDAR as ground truth to supervise the depth estimation during training, without LiDAR-Teacher supervision (only \mathcal{L}_{dp} without \mathcal{L}_T). *Input-fusion Teacher* is an alternative way of designing the LiDAR-Teacher, where we directly fuse point (x, y, z) coordinates into their corresponding image pixels as additional channels in the teacher model, similar to Pointpainting [36]. We use *DA* and *CM* to denote whether a model considers domain adaptation and cross-modality in design, respectively. Results are reported on vehicle, drivable roads, and lane marking classes using intersection-over-union (IoU).

Day-to-Night Adaptation. As shown in Table 1 on the left, we observe that our DualCross model achieves the best performance on all classes. We notice that the improvement under the Day \rightarrow Night setting is exceptionally high. This is because the initial domain gap between day and night scenarios is very large in the camera modality space. Moreover, the LiDAR sensor is robust under illumination changes, due to its active imaging mechanism as opposed to camera’s passive one. Thus, incorporating LiDAR point cloud information helps the model to learn a more robust, illumination-invariant representation from the image inputs.

Dry-to-Rain Adaptation. As shown in Table 1 on the right, under this setting we also observe that our DualCross model achieves the best performance on all classes. We no-

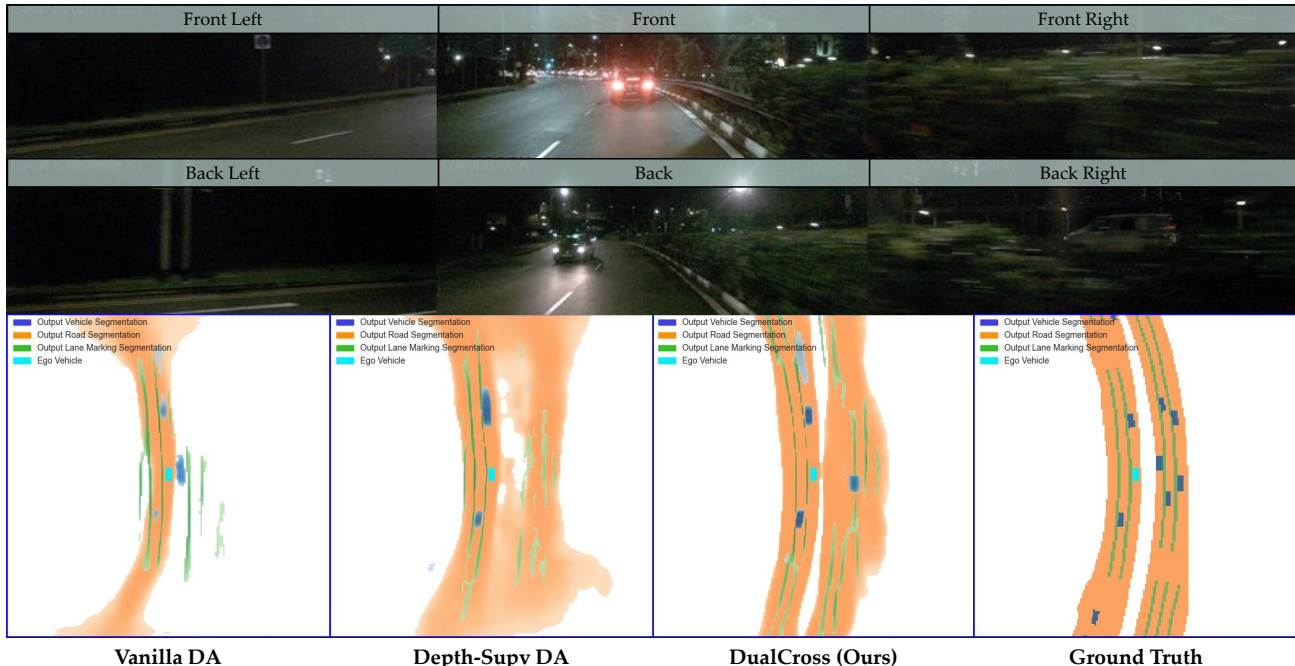


Figure 3: **Qualitative Results in Day \rightarrow Night setting** (model is trained with daytime data, and validated with night data). We notice that DualCross performs significantly better than other baselines for **vehicles**, **drivable roads**, and **lane marking** classes. From **left to right**: (1) Vanilla adversarial learning; (2) LiDAR as depth supervision with adversarial learning; (3) our DualCross model; (4) Ground Truth. Best viewed in color.

tice that the improvement under the Dry \rightarrow Rain setting is not as big as the previous setting. This is because the domain gap between dry and rain scenarios is not big in the image modality. Hence, baseline methods OFT and LSS are already able to obtain decent results even without domain adaptation. Furthermore, rainy weather is known to cause great domain shift in the LiDAR modality [45]. As a result, the knowledge learned from source-exclusive LiDAR suffers from an unknown domain shift which hinders its usefulness. This can potentially cancel out the benefit of 3D information learned from point clouds and explains for the smaller improvement.

Dataset-to-Dataset Adaptation. As shown in Table 3, we also observe that our DualCross model achieves the best performance in the nuScenes \rightarrow Lyft setting. Following [30], because Lyft does not provide road segment and lane marking information in the HD map, we report results on the vehicle class. Compared with baselines with and without domain adaptation or cross-modality learning, our DualCross demonstrates superior performance in leveraging and adapting LiDAR information.

City-to-City Adaptation. As shown in Table 2, we observe that our DualCross model achieves the best performance on all classes for two inter-city transfer settings. Without domain adaptation, baseline approaches MonoLayout, OFT, and LSS all suffer from performance degrada-

tion. Direct depth supervision and alternative input-fusion teacher models do not bring as much improvement as DualCross. The results clearly demonstrate the effectiveness of our method by distilling and aligning the LiDAR information for cross-modality 3D BEV perception.

Qualitative Results. As shown in Figure 3, under the Day \rightarrow Night domain shift setting, our model achieves significantly better monocular 3D perception than other baselines. We observe that DualCross provides more clearly defined road boundaries and lane markings. The depth and size of the vehicles and the road on the right side are also predicted more accurately. DualCross only misses some vehicles that are hardly visible in camera due to occlusion and distance. Overall, the qualitative results validate the effectiveness of DualCross in closing the gap between data domains and leveraging point clouds information for better 3D inference.

4.2. Analysis and Ablation Study

Direct LiDAR Supervision Leads to Worse Performance. It is naturally believed that introducing multiple sensors in the perception model is bound to increase the model performance. Surprisingly, experiments shown in Table 4 negate this naive intuition. When we introduce the LiDAR sensor in the source domain as depth supervision, the result decreases by 0.3. As we described in Sec. 3.2, the domain distribution divergence increases after introducing

Table 4: Our proposed components all contribute to the final performance. We report results on the vehicle class under the *day-to-night* domain gap in IoU. WA, AD, LS, LT stand for Wide Augmentation, Adversarial Discriminators, LiDAR Supervision, and LiDAR-Teacher, respectively.

Baseline	WA	AD	LS	LT	Results	diff
✓					6.7	0
✓			✓		6.4	-0.3
✓	✓				10.3	+3.6
✓	✓	✓			11.2	+4.5
✓	✓	✓	✓		15.7	+9.0
✓	✓	✓	✓	✓	17.0	+10.3

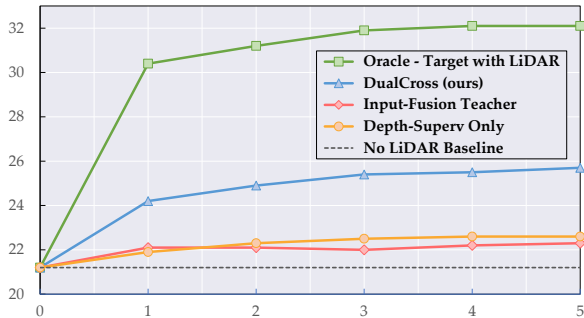


Figure 4: Results of DualCross improve as the number of LiDAR points increases.

the sensor-modality shift. As a result, we propose multiple components in DualCross to account for the visual and sensor domain shifts. Experiments show that while the wide augmentation strategy and adversarial discriminator both achieve better results than the baseline (11.2 vs. 6.7 in IoU), our LiDAR-Teacher further boosts the result to 17.0 by leveraging effective LiDAR knowledge distillation.

LiDAR Density & Comparison with Oracle Model. As shown in Figure 4, we validate that our model achieves higher performance when denser LiDAR is available. This can be accomplished by grouping continuous scans of LiDAR point clouds (from 1 to 5) into a single unit, to have a denser 3D representation of the scene. We observe that other cross-modality baselines including *Input-Fusion Teacher* and *Depth-Supv* models cannot effectively leverage the LiDAR knowledge, even with dense point clouds available. We also compare our model with the LiDAR oracle model (target domain also has the LiDAR modality) and find that the gap between the upper bound result and the No-LiDAR baseline is significantly reduced. The remaining performance gap is caused by the unknown LiDAR domain gap which we hope to further reduce in future work.

Dealing with Mixed Domain Shift. Another common but under-explored question we observe in the 3D domain adaption setting is the mixed domain shift problem, where multiple types of gaps between source and target domains occur concurrently. For example, in the nuScenes dataset,

Table 5: The proposed progressive learning strategy effectively addresses the challenge caused by the mixed domain gap scenario (*Boston-to-Singapore* mixed with *day-to-night*) on nuScenes.

Mixed Domain Gap	Vehicle	Road	Lane
Direct Inference	17.6	38.2	10.6
Vanilla DA	13.0	31.4	9.1
Progressive DA	18.8	41.5	13.2
DualCross (ours)	20.5	43.1	15.6

Table 6: DualCross achieves great perception results with efficient inference time compared with the baselines.

	#Params (M)	Frame-per-Second (FPS)
OFT [33]	22	25
LSS [30]	14	35
DualCross (Ours)	15	33

the Boston data are collected exclusively during daytime, whereas the Singapore data encompass both day and night captures. This leads to a mixture of city-wise and lighting-wise domain shifts. As shown in Table 5, we find that directly leveraging domain adaptation in this scenario leads to worse performance than direct inference, because mixed domains in the target confuse the discriminator. Hence, we propose a progressive learning mechanism, where we first perform adaptation with city-wise data for 100K steps, and then train the model on the full target domain dataset for another 150K steps. This effectively alleviates the mixed domain shift problem, and helps DualCross achieve leading results than other baselines.

Computational Complexity. Table 6 summarizes the number of parameters and inference speed for prior baselines and our model. Our Lidar-Teacher distillation and multi-level adversarial learning modules do not affect the inference efficiency of DualCross compared with the baseline. Our total number of parameters is 15M, and our inference time is 33 Frame-per-Second (FPS) on a V100 GPU, which is on par with the baseline LSS [30]. The training time for our model is around 20 hours on 4×V100 GPUs.

5. Conclusion

In this paper, we proposed DualCross to estimate 3D scene representation in BEV under domain shift and modality change. To achieve this, we construct a LiDAR-Teacher and distill knowledge from it into a Camera-Student by feature supervision. And we further propose to align feature space between the domains using multi-stage adversarial learning. Results on large-scale datasets with various challenging domain gaps demonstrated the effectiveness of our approach, which marks a significant step towards robust 3D scene perception in the wild.

References

- [1] Shai Ben-David, John Blitzer, Koby Crammer, Alex Kulesza, Fernando Pereira, and Jennifer Wortman Vaughan. A theory of learning from different domains. *Machine learning*, 79(1):151–175, 2010.
- [2] Garrick Brazil and Xiaoming Liu. M3d-rpn: Monocular 3d region proposal network for object detection. In *ICCV*, 2019.
- [3] Holger Caesar, Varun Bankiti, Alex H Lang, Sourabh Vora, Venice Erin Liong, and Qiang Xu. nuscenes: A multimodal dataset for autonomous driving. In *CVPR*, 2020.
- [4] Yigit Baran Can, Alexander Liniger, Danda Pani Paudel, and Luc Van Gool. Structured bird’s-eye-view traffic scene understanding from onboard images. In *ICCV*, 2021.
- [5] Yuhua Chen, Wen Li, Christos Sakaridis, Dengxin Dai, and Luc Van Gool. Domain adaptive faster r-cnn for object detection in the wild. In *CVPR*, 2018.
- [6] Zehui Chen, Zhenyu Li, Shiquan Zhang, Liangji Fang, et al. Bevdistill: Cross-modal bev distillation for multi-view 3d object detection. In *ICLR*, 2023.
- [7] Jang Hyun Cho and Bharath Hariharan. On the efficacy of knowledge distillation. In *ICCV*, 2019.
- [8] Zhiyu Chong, Xinzhu Ma, Hong Zhang, Yuxin Yue, Haojie Li, Zhihui Wang, and Wanli Ouyang. Monodistill: Learning spatial features for monocular 3d object detection. In *ICLR*, 2022.
- [9] Yaroslav Ganin and Victor Lempitsky. Unsupervised domain adaptation by backpropagation. In *ICML*, 2015.
- [10] Rui Gong, Dengxin Dai, Yuhua Chen, Wen Li, and Luc Van Gool. mdalu: Multi-source domain adaptation and label unification with partial datasets. In *ICCV*, 2021.
- [11] Xiaoyang Guo, Shaoshuai Shi, Xiaogang Wang, et al. Ligastereo: Learning lidar geometry aware representations for stereo-based 3d detector. In *ICCV*, 2021.
- [12] Noureldin Hendy, Cooper Sloan, Feng Tian, Pengfei Duan, Nick Charchut, Yuesong Xie, Chuang Wang, and James Philbin. Fishing net: Future inference of semantic heatmaps in grids. In *CVPR*, 2020.
- [13] Yu Hong, Hang Dai, and Yong Ding. Cross-modality knowledge distillation network for monocular 3d object detection. In *ECCV*, 2022.
- [14] Maximilian Jaritz, Tuan-Hung Vu, Raoul de Charette, Emilie Wirbel, and Patrick Pérez. xmuda: Cross-modal unsupervised domain adaptation for 3d semantic segmentation. In *CVPR*, 2020.
- [15] R. Kesten, M. Usman, J. Houston, T. Pandya, K. Nadhamuni, A. Ferreira, M. Yuan, B. Low, A. Jain, P. Ondruska, S. Omari, S. Shah, A. Kulkarni, A. Kazakova, C. Tao, L. Platinisky, W. Jiang, and V. Shet. Level 5 perception dataset 2020. <https://level-5.global/level5/data/>, 2019.
- [16] Diederik P Kingma and Jimmy Ba. Adam: A method for stochastic optimization. *arXiv preprint arXiv:1412.6980*, 2014.
- [17] Jogendra Nath Kundu, Phani Krishna Uppala, Anuj Pahuja, and R Venkatesh Babu. Adadepth: Unsupervised content congruent adaptation for depth estimation. In *CVPR*, 2018.
- [18] Yanwei Li, Yilun Chen, Xiaojuan Qi, Zeming Li, Jian Sun, and Jiaya Jia. Unifying voxel-based representation with transformer for 3d object detection. 2022.
- [19] Yin hao Li, Zheng Ge, Guanyi Yu, Jinrong Yang, Zengran Wang, Yukang Shi, Jianjian Sun, and Zeming Li. Bevdepth: Acquisition of reliable depth for multi-view 3d object detection. *arXiv*, 2022.
- [20] Yu-Jhe Li, Xiaoliang Dai, Chih-Yao Ma, Yen-Cheng Liu, Kan Chen, Bichen Wu, Zijian He, Kris Kitani, and Peter Vajda. Cross-domain object detection via adaptive self-training. *arXiv preprint arXiv:2111.13216*, 2021.
- [21] Ming Liang, Bin Yang, Yun Chen, Rui Hu, and Raquel Urtasun. Multi-task multi-sensor fusion for 3d object detection. In *CVPR*, 2019.
- [22] Zhipeng Luo, Zhongang Cai, Changqing Zhou, Gongjie Zhang, Haiyu Zhao, Shuai Yi, Shijian Lu, Hongsheng Li, Shanghang Zhang, and Ziwei Liu. Unsupervised domain adaptive 3d detection with multi-level consistency. In *ICCV*, 2021.
- [23] Yunze Man, Xinshuo Weng, Prasanna Kumar Sivakumar, Matthew O’Toole, and Kris M Kitani. Multi-echo lidar for 3d object detection. In *ICCV*, 2021.
- [24] Kaustubh Mani, Swapnil Daga, Shubhika Garg, Sai Shankar Narasimhan, Madhava Krishna, and Krishna Murthy Jatavallabhula. Monolayout: Amodal scene layout from a single image. In *WACV*, 2020.
- [25] Seyed Iman Mirzadeh, Mehrdad Farajtabar, Ang Li, Nir Levine, Akihiro Matsukawa, and Hassan Ghasemzadeh. Improved knowledge distillation via teacher assistant. In *AAAI*, 2020.
- [26] Bowen Pan, Jiankai Sun, Ho Yin Tiga Leung, Alex Andonian, and Bolei Zhou. Cross-view semantic segmentation for sensing surroundings. *RA-L*, 2020.
- [27] Jinhyung Park, Xinshuo Weng, Yunze Man, and Kris Kitani. Multi-modality task cascade for 3d object detection. In *BMVC*, 2021.
- [28] Adam Paszke, Sam Gross, Francisco Massa, Adam Lerer, James Bradbury, Gregory Chanan, Trevor Killeen, Zeming Lin, Natalia Gimelshein, Luca Antiga, et al. Pytorch: An imperative style, high-performance deep learning library. In *NeurIPS*, 2019.
- [29] Duo Peng, Yinjie Lei, Wen Li, Pingping Zhang, and Yulan Guo. Sparse-to-dense feature matching: Intra and inter domain cross-modal learning in domain adaptation for 3d semantic segmentation. In *ICCV*, 2021.
- [30] Jonah Philion and Sanja Fidler. Lift, splat, shoot: Encoding images from arbitrary camera rigs by implicitly unprojecting to 3d. In *ECCV*, 2020.
- [31] Charles R Qi, Xinlei Chen, Or Litany, and Leonidas J Guibas. Imvotenet: Boosting 3d object detection in point clouds with image votes. In *CVPR*, 2020.
- [32] Can Qin, Haoxuan You, Lichen Wang, C-C Jay Kuo, and Yun Fu. Pointdan: A multi-scale 3d domain adaption network for point cloud representation. In *NeurIPS*, 2019.
- [33] Thomas Roddick, Alex Kendall, and Roberto Cipolla. Orthographic feature transform for monocular 3d object detection. *arXiv preprint arXiv:1811.08188*, 2018.

- [34] Pei Sun, Henrik Kretschmar, Xerxes Dotiwalla, Aurelien Chouard, Vijaysai Patnaik, Paul Tsui, James Guo, Yin Zhou, Yuning Chai, Benjamin Caine, et al. Scalability in perception for autonomous driving: Waymo open dataset. In *CVPR*, 2020.
- [35] Mingxing Tan and Quoc Le. Efficientnet: Rethinking model scaling for convolutional neural networks. In *ICML*, 2019.
- [36] Sourabh Vora, Alex H Lang, Bassam Helou, and Oscar Beijbom. Pointpainting: Sequential fusion for 3d object detection. In *CVPR*, 2020.
- [37] Tai Wang, ZHU Xinge, Jiangmiao Pang, and Dahua Lin. Probabilistic and geometric depth: Detecting objects in perspective. In *CoRL*, 2022.
- [38] Tai Wang, Xinge Zhu, Jiangmiao Pang, and Dahua Lin. Fcos3d: Fully convolutional one-stage monocular 3d object detection. In *ICCV*, 2021.
- [39] Yan Wang, Wei-Lun Chao, Divyansh Garg, Bharath Hariharan, Mark Campbell, and Kilian Q Weinberger. Pseudo-lidar from visual depth estimation: Bridging the gap in 3d object detection for autonomous driving. In *CVPR*, 2019.
- [40] Yue Wang and Justin M Solomon. Object dgcnn: 3D object detection using dynamic graphs. In *NeurIPS*, 2021.
- [41] Xinshuo Weng and Kris Kitani. Monocular 3d object detection with pseudo-lidar point cloud. In *ICCVW*, 2019.
- [42] Xinshuo Weng, Yongxin Wang, Yunze Man, and Kris M Kitani. Gnn3dmot: Graph neural network for 3d multi-object tracking with 2d-3d multi-feature learning. In *CVPR*, 2020.
- [43] Bichen Wu, Xuanyu Zhou, Sicheng Zhao, Xiangyu Yue, and Kurt Keutzer. Squeezesegv2: Improved model structure and unsupervised domain adaptation for road-object segmentation from a lidar point cloud. In *ICRA*, 2019.
- [44] Bin Xu and Zhenzhong Chen. Multi-level fusion based 3d object detection from monocular images. In *CVPR*, 2018.
- [45] Qiangeng Xu, Yin Zhou, Weiyue Wang, Charles R Qi, and Dragomir Anguelov. Spg: Unsupervised domain adaptation for 3d object detection via semantic point generation. In *ICCV*, 2021.
- [46] Xu Yan, Jiantao Gao, Chaoda Zheng, Chao Zheng, Ruimao Zhang, Shuguang Cui, and Zhen Li. 2dpass: 2d priors assisted semantic segmentation on lidar point clouds. In *ECCV*, 2022.
- [47] Jihan Yang, Shaoshuai Shi, Zhe Wang, Hongsheng Li, and Xiaojuan Qi. St3d: Self-training for unsupervised domain adaptation on 3d object detection. In *CVPR*, 2021.
- [48] Jin Hyeok Yoo, Yeocheol Kim, Ji Song Kim, and Jun Won Choi. 3d-cvf: Generating joint camera and lidar features using cross-view spatial feature fusion for 3d object detection. In *ECCV*, 2020.
- [49] Weichen Zhang, Wen Li, and Dong Xu. Srdan: Scale-aware and range-aware domain adaptation network for cross-dataset 3d object detection. In *CVPR*, 2021.
- [50] Shanshan Zhao, Huan Fu, Mingming Gong, and Dacheng Tao. Geometry-aware symmetric domain adaptation for monocular depth estimation. In *CVPR*, 2019.
- [51] Ming Zhu, Chao Ma, Pan Ji, and Xiaokang Yang. Cross-modality 3d object detection. In *WACV*, 2021.
- [52] Yichen Zhu and Yi Wang. Student customized knowledge distillation: Bridging the gap between student and teacher. In *ICCV*, 2021.

A. Dataset Details

In this section, we explain our dataset split in more details. For our experiments, we always split the target domain into two subsets for a fair comparison. One of them can be accessed during training for adversarial learning and domain alignment, and the other is held out exclusively for validation.

City-to-City Adaptation. For the *city-to-city* adaptation scenario, we sub-sample the trainval split of the large-scale dataset nuScenes [3] captured in Boston and Singapore cities. We treat one city as the source domain and the other as the target domain. The Boston part of data has 467 scenes in total, which is separated into 350 scenes for training and 117 scenes for validation. And the Singapore part of data has 383 scenes in total, which is separated into 287 scenes for training and 96 scenes for validation.

Day-to-Night Adaptation. For the *day-to-night* adaptation scenario, we also sub-sample the trainval split of the large-scale dataset nuScenes [3]. Every scene in the nuScenes dataset has a sentence of description, which can be parsed and used to categorize it into certain class. In this way, we create a day scene subset and a night scene subset out of the whole dataset. We treat day as the source domain and night as the target domain, because the night subset has significantly fewer samples than the day subset. The day split has 751 scenes which are all used for training. And the night part has 99 scenes in total, which is separated into 74 scenes for training and 25 scenes for validation.

Dry-to-Rain Adaptation. For the *dry-to-rain* adaptation scenario, we also sub-sample the trainval split of the large-scale dataset nuScenes [3]. Similarly, using the scene description sentence, we create a dry (non-rainy) scene subset and a rainy scene subset out of the whole dataset. We treat dry as the source domain and rain as the target domain, because the rain subset has significantly fewer samples than the dry subset. The dry split has 685 scenes which are all used for training. And the rain part of data has 165 scenes in total, which is separated into 124 scenes for training and 41 scenes for validation.

Dataset-to-Dataset Adaptation. For the *dataset-to-dataset* adaptation scenario, we use the two large-scale autonomous driving datasets nuScenes [3] and Lyft [15]. We treat one dataset as the source domain and the other as the target domain. For the nuScenes dataset, we use the original train and validation split, which has 700 scenes and 150 scenes, respectively. The Lyft dataset does not have an original split, so we sub-sample 132 scenes for training and 48 scenes for validation.

B. Additional Results and Analysis

B.1. Unique Challenge Due to Problem Formulation

We provide another perspective to understand the challenges brought by the co-existence of cross-modality and cross-domain gaps, thus further motivating the design of our architecture. It is proved that in domain adaptation, the target domain error $\epsilon^t(h)$ for input h can be upper-bounded by the inequality [1]:

$$\epsilon^t(h) \leq \epsilon^s(h) + d_{\mathcal{H}\Delta\mathcal{H}}(P_X^s, P_X^t) + C, \quad (6)$$

where the bound is composed of the source-domain error $\epsilon^s(h)$, source-target distribution divergence $d_{\mathcal{H}\Delta\mathcal{H}}(P_X^s, P_X^t)$, and another term which is considered constant in our case. Existing domain adaptation work mostly focuses on reducing the source-domain error. However, while the introduction of the LiDAR sensor **reduces the first term, it increases the second term**, because the source and target domains have an additional sensor-type gap. It is also demonstrated in Sec. 4 that naively using source domain LiDAR can even hinder the target performance rather than improve it. Hence, the unique difficulty of our work lies in *leveraging LiDAR to reduce the source-domain error $\epsilon^s(h)$ and, in the meanwhile, preventing distribution divergence $d_{\mathcal{H}\Delta\mathcal{H}}(P_X^s, P_X^t)$ from increasing too much.*

B.2. Different Depth GT Signal Generation Methods

As shown in Table 7, we validate DualCross’s design choice in depth ground truth signal generation (Eq. 1 in the main paper) by comparing with different alternative methods. Note that all the methods have the same output when there is no point or only one point projected to a pixel. The difference only comes from the behaviour when multiple points are projected to one pixel.

- *Majority Voting* means to generate a one-hot GT vector by assigning “1” to the depth bin with the most number of points inside, and randomly select one bin when more than one bin with the most number of points.
- *Random Selection* means to generate a one-hot GT vector by randomly selecting one of all the projected points, and assigning “1” to the depth bin in which the selected point lies.
- *Softmax Point Number Distribution* means to count the number of points inside every depth bin, and then use softmax to turn this vector into a distribution.

Finally, in DualCross we use direct *Point Number Distribution*, where we count the number of points inside every depth bin, and divide the vector by the total number

Table 7: We validate the design choices of DualCross by comparing with various depth GT generation methods and different choices of teacher supervision signals. Results show that depth supervision generated by Point Number Distribution (Eq. 1 in the main paper), and feature-level supervision from LiDAR-Teacher helps the model achieve the best performance.

Design choices in Day \rightarrow Night Setting		Vehicle	Road	Lane
Depth Ground Truth Signal (From Point Clouds)	No LiDAR	11.2	48.8	11.1
	Majority Voting	14.1	50.0	13.7
	Random Selection	13.8	49.5	12.6
	Softmax Point Number Distribution	13.1	49.9	11.9
	Point Number Distribution (Ours)	17.0	51.8	16.9
LiDAR-Teacher Supervision	No LiDAR-Teacher	15.7	50.5	14.2
	Soft-label Supervision	15.2	50.7	13.9
	Feature Supervision (Ours)	17.0	51.8	16.9

of points to get a depth distribution. Results show that our direct point number distribution outperforms other counterparts in ground truth generation. One possible reason is because DualCross down-samples the feature map $8\times$ when estimating the 3D depth volume. This makes it much more common for multiple points with different depth values to fall in the same pixel. By contrast, the other two methods, *Majority Voting* and *Random Selection*, will lose valuable information in these cases. On the other hand, softmax activation over-smooths the distribution, and also assigns small values to zero bins (depth bins with no point inside). Hence, we find that preserving the native depth distribution of the points is better to supervise DualCross in 3D evaluation.

B.3. Different LiDAR-Teacher Supervision Design

As shown in Table 7, we also validate DualCross’s design choice of LiDAR-Teacher Supervision by comparing with different alternative methods. In addition to the feature-level supervision used in DualCross, another commonly used teacher supervision is the soft label output. Specifically, *Soft-label Supervision* means to use the class distribution output of the teacher model as the supervision of the student model, as opposed to the one-hot vector from the ground truth annotation. We find that the feature-level supervision performs better than the soft-label supervision. One reason is because we use a small number of classes, which makes the supervision from the soft labels less informative. Moreover, because the teacher and student models in DualCross have almost identical architecture and capacity, enforcing the corresponding feature level similarity between the teacher and student models provides a stronger supervision than the soft-label output, without harming the model learning. As future work, we will explore whether soft labels may be more useful when the number of classes in the model is larger.

B.4. Lyft-to-nuScenes Adaptation

Due to page limit, Table 3 in the main paper only shows the results under the nuScenes \rightarrow Lyft setting. Here we also

Table 8: DualCross achieves the best performance on all classes under *Lyft-to-nuScenes* domain gaps in IoU. *DA* and *CM* mean domain adaptation and cross modality, respectively.

Lyft \rightarrow nuScenes	DA	CM	Vehicle
MonoLayout [24]	\times	\times	7.1
OFT [33]	\times	\times	11.9
LSS [30]	\times	\times	13.8
Wide-range Aug.	\checkmark	\times	14.6
Vanilla DA	\checkmark	\times	15.1
Depth-Supv DA	\checkmark	\checkmark	16.5
Input-fusion Teacher	\checkmark	\checkmark	15.1
DualCross (ours)	\checkmark	\checkmark	19.2

present the results under the Lyft \rightarrow nuScenes adaptation setting for completeness. As shown in Table 8, we can also observe that our DualCross model achieves the best performance. Like previous scenarios, the baseline approaches, MonoLayout, OFT, and LSS without domain adaptation suffer from performance degradation due to domain shift. And compared with other baselines with domain adaptation or cross-modality learning, our DualCross performs better in leveraging and adapting LiDAR information.

B.5. Effect of Designs on Different Domain Gaps

We find in our experiments that different types of domain gaps react unevenly to different model designs. As shown in Table 9, for the Day \rightarrow Night setting which has less domain shift in the LiDAR point cloud modality than the camera modality, the depth supervision and the middle layer feature alignment block provide a large improvement on top of other modules. By contrast, under the Dry \rightarrow Rain setting, where domain gap is larger for point clouds than images, no significant improvement is achieved by using these two components. This further validates the necessity of using multiple modalities under domain adaptation settings, which can effectively improve the algorithm robustness under different domain shifts.

Table 9: Different types of domain gaps react unevenly to different model designs. Direct depth supervision and the middle layer feature alignment block provide a larger improvement under the Day \rightarrow Night setting than the Dry \rightarrow Rain setting.

DualCross Designs	Day \rightarrow Night	Dry \rightarrow Rain
Image-only Baseline	11.2	28.3
LiDAR Teacher Feature Supervision	14.9 (+3.7)	29.5 (+1.2)
LiDAR Teacher Feature + Depth Supervision	17.0 (+5.8)	29.6 (+1.3)
Without Domain Alignment	7.1	28.1
Feature Alignment at Final layer	12.2 (+5.1)	29.6 (+1.5)
Feature Alignment at Mid + Final layer	17.0 (+9.9)	29.3 (+1.2)

Table 10: DualCross achieves the best performance under simultaneous modality and domain shift for 3D object detection. Domain shift is **Singapore** \rightarrow **Boston**.

Modality-shift + Domain Shift	mAP \uparrow	NDS \uparrow
LSS [30]	16.0	20.3
MonoDistill [8]	16.5	21.9
Depth-Supv DA	19.1	23.5
DualCross	22.5	26.1

B.6. 3D Detection Results and Comparisons

Baselines. In addition to the BEV segmentation task, we compare DualCross with state-of-the-art cross-modality 3D object detection models, MonoDistill [8] and Set2Set [40]. The original MonoDistill was designed for the single-camera setting on the KITTI dataset, so we extend it into a multi-camera setting for a fair comparison. We evaluate with mean Average Precision (mAP) and Nuscenes Detection Score (NDS) metrics [3].

Modality-Shift + Domain-Shift. As shown in Table 10, under concurrent modality and domain gaps, DualCross outperforms all previous baselines by a large margin, showing that it is a more robust and trustworthy model in real-world scenarios.

Modality-Shift Only. As shown in Table 11 on the right, our DualCross model achieves the best performance. By using ResNet-50, the same image feature extractor backbone as MonoDistill, we can achieve more than 1% improvement in mAP and NDS metrics. Moreover, our model still runs 42ms per frame during inference, faster than MonoDistill which runs 80ms per frame.

B.7. Solving Scale Problem

Scale ambiguity is an inherent problem for monocular depth estimation. We solve this problem by using the random cropping and scaling augmentation strategy during training, and also by matching the FoV (Field-of-View) of two domains using their intrinsic matrices. The augmentation increases the robustness of the depth prediction model

Table 11: DualCross achieves great performance under only the modality shift for 3D object detection. EfficientNet and ResNet50 are backbones for image feature extraction.

Modality-shift Only	mAP \uparrow	NDS \uparrow
Set2Set [40]	33.1	41.0
MonoDistill [8]	34.3	41.2
DualCross-EfficientNet	34.5	41.5
DualCross-ResNet50	35.2	42.4

Table 12: DualCross achieves great performance with scaling augmentation and FoV matching for *nuScenes-to-Lyft* domain gaps in vehicle IoU.

nuScenes \rightarrow Lyft	Scaling Aug.	Match FoV	Vehicle IoU
None			23.5
with scaling aug.	✓		23.8
with both	✓	✓	24.4

in scale difference. And the FoV matching scales the images in the target domain to match the FoV of the source domain. This ensures that one object looks approximately the same size across images, if it is of the same distance to the ego vehicle in source and target domains, thus reducing the scale ambiguity. In Table 12, we provide an ablation study of scale augmentation and FoV matching in nuScenes-to-Lyft adaptation. As we can see, they both improve our final model performance.

From Table 12, we also notice that even without the two methods mentioned above, the model still performs fairly well, compared with the baseline methods in Table 3. This is because in driving scenarios, the camera FoV, the context in the images, and the depth distribution of the images have a relatively strong prior – they do not have a strong discrepancy even across different driving scenarios (domains). This is different from more general depth estimation scenarios, where objects can have drastically different depth distribution and the intrinsic matrix can have big differences from image to image.

Table 13: Our proposed modules achieve great performance in both depth estimation and semantic segmentation tasks.

Day → Night	Depth Estimation (CEE)	Semantic Segmentation (IoU)
Direct Inference	2.56	27.5
Adversarial Learning (AL)	1.97	31.8
Lidar-Teacher Supervision + AL	1.41	32.1

Table 14: Naive LiDAR supervision cannot help the final perception under cross-domain and cross-modality scenarios.

Method	Boston → Singapore	Dry → Rain	nuScenes → Lyft
LSS [30] Baseline	17.5	27.9	20.6
Baseline + naïve LiDAR supervision	17.5 (-0.0)	28.2 (+0.3)	20.3 (-0.2)
DualCross (Full Model)	20.5 (+3.0)	29.6 (+1.7)	24.4 (+3.9)

B.8. Ablation in Semantic Segmentation and Depth Prediction

From the task perspective, there are two domain gaps in this task, one in the semantic segmentation task and the other in the depth prediction task. In Table 13, we show the result of depth estimation and semantic segmentation alone in the Day-to-Night scenario.

For depth estimation, we report the cross-entropy error (CEE) with the ground truth we described in Sec 3.2, because each pixel will have multiple depth values. For this task, the LiDAR teacher supervision refers to L_{dp} in our main pipeline. We observe that our method significantly improves the depth estimation metrics by 44.9%.

For semantic segmentation, we report the IoU for the vehicle class. To remove the effect of depth estimation, we use a pre-trained depth estimation model and fix its weight. For this task, the LiDAR teacher supervision refers to L_T in our main pipeline. We observe that the DualCross architecture also improves the baseline method by 16.7%.

B.9. Results of Naive LiDAR Supervision Under Other Adaptation Settings

In Table 14, we present the ablation study of direct LiDAR supervision under different adaptation scenarios. We observe that in all scenarios, naive LiDAR supervision cannot lead to better performance against the baseline.

When the source and target domains have larger visual gaps (Day→Night, nuScenes→Lyft), the naive supervision leads to worse results, and when the gap is smaller (Boston→Singapore, Dry→Rain), the LiDAR supervision results in on-par or only slightly better performance. The reason is that although the LiDAR sensor in the source domain provides 3D knowledge to the model, it also increases the domain discrepancy between the source and the target (the model has to adapt to the additional modality shift), which hurts the model performance instead.

C. Visualization on Failure Cases

As shown in Figure 5, we visualize the failure cases of our DualCross model. We notice that most failure cases come from far distance, or heavy occlusion (which are typical failure cases for baselines as well). Faraway objects are known to be typically hard cases for monocular 3D perception [44, 39, 2, 38, 37], because the ambiguity of object depth from images becomes larger as the distance increases. This can be potentially alleviated by using a smaller down-sampling rate when extracting the image features. As for objects inside the red dashed boxes in Figure 5, they can be seen in the LiDAR sensor due to the higher deployment position. But in cameras, the objects are almost invisible due to the occlusion of vegetation, structures, or other vehicles. The occlusion problem can be potentially addressed if we have access to additional sensors during evaluation. As future work, we will also try to alleviate the occlusion problem in monocular settings by leveraging temporal information.

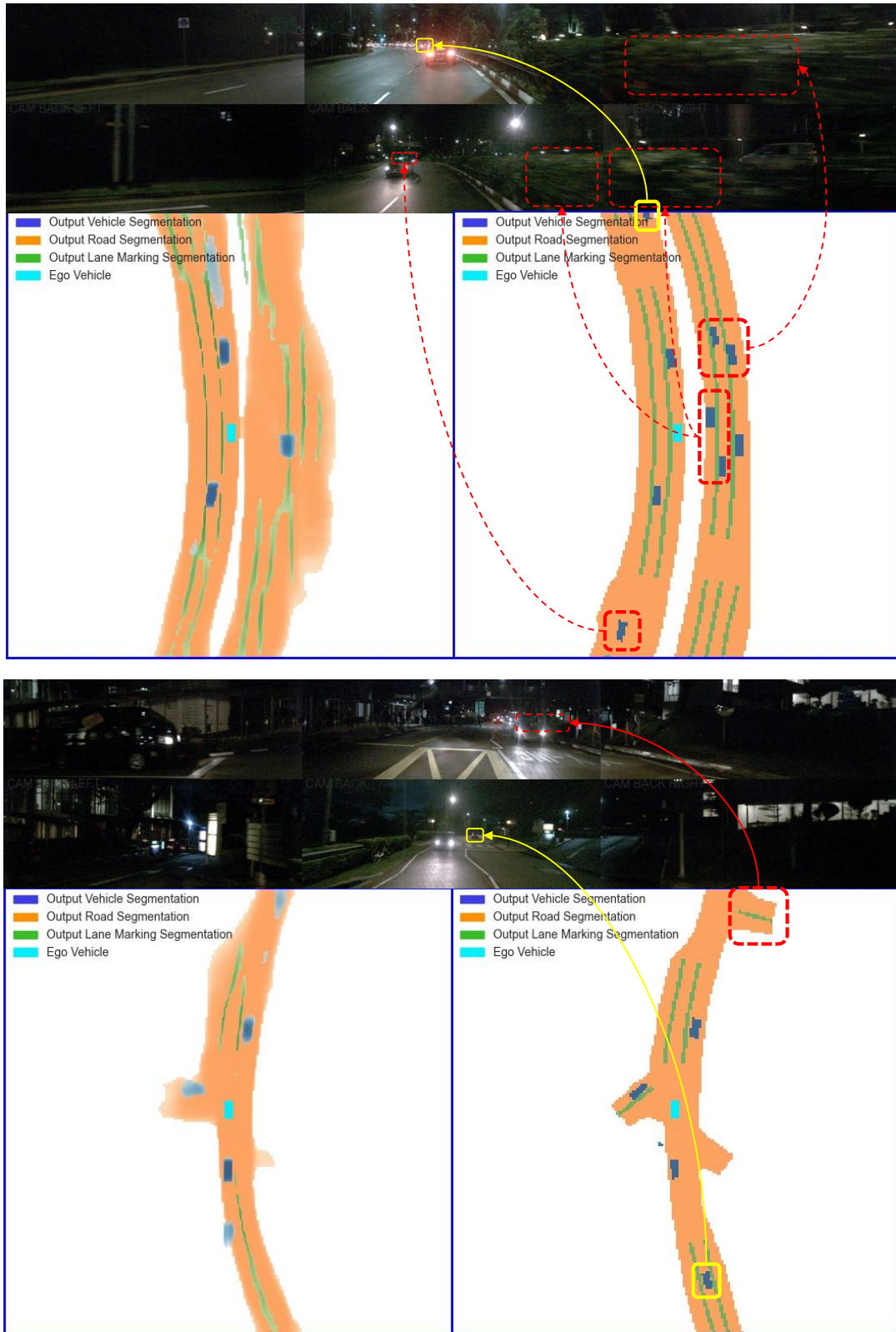


Figure 5: **Visualization of failure cases of DualCross** (model is trained with daytime data, and validated with night data).
 Up: Input images. Left: Prediction from DualCross. Right: Ground truth. We notice that major failure cases of DualCross are far distance and occlusions of objects and regions.